THE JOURNAL OF PHYSICAL CHEMISTRY C

Article

Cite This: J. Phys. Chem. C 2018, 122, 24085−24093

pubs.acs.org/JPCC

Direct Imaging of Atomic-Scale Surface Structures of Brookite TiO_2 Nanoparticles by Frequency Modulation Atomic Force Microscopy in Liquid

Hitoshi Asakawa,[†,‡,§] Eero Holmström,[∥] Adam S. Foster,[*,‡,∥,⊥] Sunao Kamimura,[#] Teruhisa Ohno,[#,¶] and Takeshi Fukuma[*,‡,¶,▽]

[†]Division of Material Chemistry, [‡]Nano Life Science Institute (WPI-NanoLSI), and [▽]Division of Electrical Engineering and Computer Science, Kanazawa University, Kakuma-machi, Kanazawa 920-1192, Japan

[§]PRESTO, Japan Science and Technology Agency, Honcho, Kawaguchi 332-0012, Japan

[∥]COMP Centre of Excellence, Department of Applied Physics, Aalto University, Helsinki FI-00076, Finland

[⊥]Graduate School Materials Science, Staudinger Weg 9, Mainz 55128, Germany

[#]Applied Chemistry Section, Department of Materials Science, Faculty of Engineering, Kyushu Institute of Technology, Kitakyushu, Fukuoka 840-8550 Japan

[¶]ACT-C, Japan Science and Technology Agency, Honcho, Kawaguchi 332-0012, Japan

Supporting Information

ABSTRACT: Direct imaging of atomic-scale surface structures of TiO_2 nanoparticles is a promising method for understanding the detailed mechanism of their photocatalytic activities. Atomic force microscopy (AFM) is one of the analytical tools used for direct imaging of surfaces, but atomic-scale AFM studies of TiO_2 nanoparticles in liquid have not been reported. Here, we report two methods for fixing of TiO_2 nanocrystals: an electrostatic method and a cross-linking method. Both methods enabled visualization of subnanoscale surface structures of brookite TiO_2 nanoparticles in liquid by frequency modulation AFM (FM-AFM). The FM-AFM imaging results and density functional theory molecular dynamics calculations suggest that the subnanoscale structures in the FM-AFM images can be explained by the arrangement of the surface topmost atoms or their hydration structures on the brookite TiO_2(210) surface. Our results open up various possibilities for studying atomic-scale surface structures of nanoparticles in liquids by AFM.

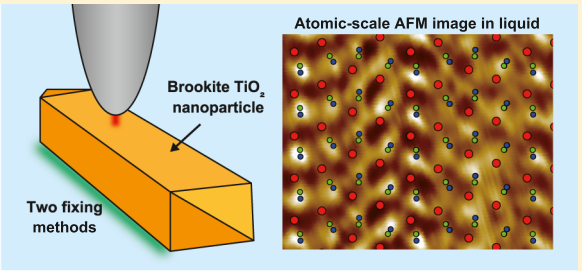

INTRODUCTION

Titanium dioxide (TiO_2) is attracting attention as a photocatalyst for many applications such as environmental cleanup[1,2] and the synthesis of useful chemicals.[3,4] The thermal stability and the photocatalytic activity of TiO_2 in water broaden its potential range of practical applications. Electron microscopy and X-ray diffraction (XRD) are the main techniques used for investigating the crystal structures of TiO_2.[5−14] Although such techniques can be used to determine precise crystal structures and their orientations, they cannot provide detailed structural information on surface structures. Investigations of the surfaces of TiO_2 are important for understanding the mechanisms of photocatalytic reactions. Scanning probe microcopy (SPM) techniques such as scanning tunneling microscopy and atomic force microscopy (AFM) enable visualization of the atomic-scale surface structures of various crystals, as previously reported.[15,16] Rutile, anatase, and brookite are the major stable polymorphs of TiO_2 crystals.[11,17−19] Early SPM studies of TiO_2 were mainly performed on crystals of rutile, which is the most stable TiO_2 crystal phase.[20−37] In addition, there have been several reports of atomic-scale investigations of anatase TiO_2 by AFM in vacuum.[38] However, the surface structure of brookite TiO_2 has not yet been experimentally investigated by SPM techniques. The atomic-scale surface structures expected from the bulk X-ray crystallography or MD simulation have not been confirmed by any microscopic experiments.

One of the major reasons for the lack of SPM investigations of brookite TiO_2 surfaces is that high-quality crystals of brookite TiO_2 are more difficult to prepare than rutile and anatase crystals. Recently, methods for preparing high-purity brookite nanocrystals have been established by using appropriate precursors, additives, and synthetic conditions.[6,8−10,12−14,39,40] Methods for controlling the particle shape and exposed facets of brookite TiO_2 nanocrystals have also been developed for improving the photocatalytic activity.[5] An understanding of the atomic-scale surface structures of

Received: July 2, 2018
Revised: September 11, 2018
Published: October 3, 2018

DOI: 10.1021/acs.jpcc.8b06262
J. Phys. Chem. C 2018, 122, 24085−24093

brookite TiO_2 is needed to clarify the relationship between the surface structures and the photocatalytic activity. The development of methods for synthesizing high-quality crystals of brookite TiO_2 has enabled examination of surfaces by SPM techniques. Investigation of the surface structures of brookite TiO_2 at an atomic resolution should contribute to our understanding of the mechanisms of photocatalytic reactions.

In this study, a laboratory-built apparatus for frequency modulation AFM (FM-AFM)[41−43] was used to investigate the atomic-scale surface structures of brookite TiO_2 in water. FM-AFM imaging in liquids has been used for various samples, ranging from inorganic crystals[44,45] to biomolecules.[46,47] As mentioned above, atomic-scale AFM investigations of rutile and anatase TiO_2 in vacuum have already been reported. However, although AFM images with atomic-scale striped contrasts obtained at the rutile (110) surface in liquid have been reported,[48] the contrasts within each stripe were not clear enough to allow their detailed comparison with an atomic surface model. To the best of our knowledge, there has been no report of atomic-scale AFM studies of TiO_2 surfaces in liquids, not only of brookite, but also of rutile and anatase.

The spatial resolution of previously reported FM-AFM images obtained in liquids suggests that atomic-scale visualization of brookite TiO_2 surfaces is a promising approach. However, there are practical problems to be overcome. At present, brookite TiO_2 can be prepared only in the form of nanoparticles, but atomic-scale SPM imaging of nanometer-sized particles is generally challenging. This is because nanocrystals are often removed from the substrate by coming into contact with the tip during scanning. In particular, the use of a stiff cantilever and a small-amplitude cantilever vibration, which are required for atomic-resolution FM-AFM imaging, makes it difficult to avoid this problem. To suppress the desorption of brookite TiO_2 nanoparticles, they need to be fixed on a substrate by strong interactions. AFM samples that consist of micrometer-sized particles can be fixed with glue.[49] However, this is not applicable to nanoparticles because they become buried in the glue layer. So far, successful atomic-scale imaging of nanoparticles has been reported only for ionic crystals grown on a substrate.[50] However, this is not applicable to TiO_2 nanoparticles because they are insoluble in water.

In this study, we investigated the atomic-scale surface structure of brookite TiO_2 nanocrystals by FM-AFM in liquid. We established two fixing methods for atomic-scale FM-AFM imaging of TiO_2 nanocrystals: an electrostatic method and a cross-linking method. Using two fixing methods, direct visualizations of atomic-scale features at brookite−water interfaces on nanoparticles were achieved. The obtained atomic-scale FM-AFM images allowed us to precisely compare them with the atomic-scale surface model. In addition, density functional theory molecular dynamics (DFT MD) simulations of the brookite TiO_2−water interface were performed to clarify the origin of the atomic-scale contrasts in FM-AFM images obtained in liquid.

EXPERIMENTAL SECTION

Synthesis of Brookite TiO_2 Nanorods. Brookite nanorods were prepared by a previously reported procedure.[51,52] Titanium(IV) ethoxide (10 g) was dissolved in ethanol (50 mL) and then deionized water (3 mL) was added to the solution. The solution was stirred for 30 min and then the precipitate was collected by centrifugation. Amorphous TiO_2 was obtained by drying the collected precipitates in a vacuum oven. Amorphous TiO_2 (4 g) was added to a solution containing 30% H_2O_2 (40 mL) and 28% NH_3 (10 mL) under cooling with water. The dispersion was stirred for 2 h and then glycolic acid (2 g) was added. The dispersion changed the color yellow to red. Stirring for 24 h to eliminate excess H_2O_2 and NH_3(aq) gave a glycolated TiO_2 complex solution. The volume and pH of the complex solution were adjusted to 50 mL and 10, respectively with NH_3 and deionized water. The solution was placed in a Teflon-lined autoclave reactor. The reactor was heated in an oven at 200 °C for 25 h. The solid substrate was separated by centrifugation, washed several times with deionized water, and dried in a vacuum oven. Crystal structures of the prepared brookite TiO_2 nanorods were confirmed with XRD measurement and SEM imaging (see Figures S1 and S2).

Zeta Potential Measurement. Aqueous suspensions of brookite TiO_2 nanorods (1.0 mg/mL) with various pH values were used for zeta potential measurements. The pH values of the aqueous suspensions were adjusted by adding hydrochloric acid to the neutral suspension. Thus, the salt concentrations of the suspensions depend on the pH conditions. For example, the estimated concentration of hydrochloric acid at pH 2 was lower than 10 mM. Measurements were performed with a Zetasizer Nano ZS instrument (Malvern Instruments, UK). The aqueous suspensions were sonicated for 1 min before the zeta potential measurements were performed.

AFM Sample Preparation by Electrostatic Method. TiO_2 nanorods were fixed by using an electrostatic method as follows. We prepared aqueous suspensions (1.0 mg/mL) of TiO_2 with the same condition as for zeta potential measurements. A suspension of TiO_2 (200 μL) was sonicated for 1 min and deposited on a freshly cleaved mica surface (a round disc of diameter 12 mm, purchased from SPI Supplies). The sample was incubated for 1 h at room temperature and rinsed with KCl aqueous solution (100 mM).

AFM Sample Preparation by Cross-Linking Method. TiO_2 nanorods were fixed by cross-linking with a phosphate-terminated self-assembled monolayer (SAM). An Au(111) substrate was prepared according to a previously reported procedure.[53] After opening the vacuum chamber to the atmosphere, the Au(111) substrate was immediately immersed in an ethanol solution of 12-mercaptododecylphosphonic acid (745855, Sigma-Aldrich) to form a SAM and left overnight in the dark. The phosphate-SAM substrate was rinsed with ethanol and pure water and then dried with N_2 gas. A suspension of brookite TiO_2 nanorods (2.0 mg/mL) was prepared with ultra-pure ethanol (Wako Pure Chemical Industries, Ltd.). After sonication for 1 min, the suspension (50 μL) was dropped on a substrate with the phosphate SAM (diameter: 12 mm) and left to stand for 1 h in a sealed vessel to suppress evaporation. After removal of unadsorbed nanorods by rinsing with ethanol, the substrate was heated at 120 °C for 24 h and cooled to room temperature. The substrate was rinsed with a KCl aqueous solution (100 mM) before the AFM measurements.

FM-AFM Measurement in Liquid. The AFM measurements were performed with a laboratory-built ultralow-noise deflection sensor as previously reported.[41−43] The laboratory-built AFM apparatus was combined with a commercially available AFM controller (Nanonis RC-4, SPECS Zurich GmbH, Zurich, Switzerland). All AFM investigation of the brookite TiO_2 nanorods were performed at room temperature in 0.1 M KCl aqueous solution. The high salt concentration

DOI: 10.1021/acs.jpcc.8b06262
J. Phys. Chem. C 2018, 122, 24085−24093

(0.1 M) can help us to obtain subnanometer-scale resolution in the FM-AFM imaging by suppressing the long-range tip−sample interaction force. In this way, we can enhance the relative contribution of the short-range tip−sample interaction force to the contrast formation in the FM-AFM images. A commercially available silicon cantilever (PPP-NCHAuD, Nanoworld, Switzerland) with a nominal spring constant of 42 N/m and a resonance frequency of 150 kHz in liquid was used. The tip side of the cantilever was coated with Si (thickness: 30 nm) by using a dc sputter coater (K575XD, Emitech), before each AFM measurement, to improve the reproducibility of atomic-resolution AFM imaging in liquid as previously reported.[54]

DFT MD Simulation. Accurate modeling of the solid−liquid interface between brookite and water, and hence the hydration structure of the crystal, was achieved by dispersion-corrected DFT calculations. Exchange−correlation effects were described by the generalized gradient approximation level Perdew−Burke−Ernzerhof (PBE)[55] functional augmented by the Grimme D3 dispersion correction.[56] All DFT calculations were performed using the CP2K package.[57] Further details of the simulation methods are available in a previous report.[52]

RESULTS AND DISCUSSION

The brookite TiO_2 nanocrystals used in this study were rod shaped with their {210} and {212} surfaces exposed, as shown in Figure 1a. We synthesized the brookite TiO_2 nanorods with the procedure that we previously reported.[51,52] Figure 1b shows the atomic-scale surface structures of the (210) brookite TiO_2 surface. In this study, we propose two methods to fix the brookite TiO_2 nanorods on a substrate for atomic-resolution FM-AFM measurements.

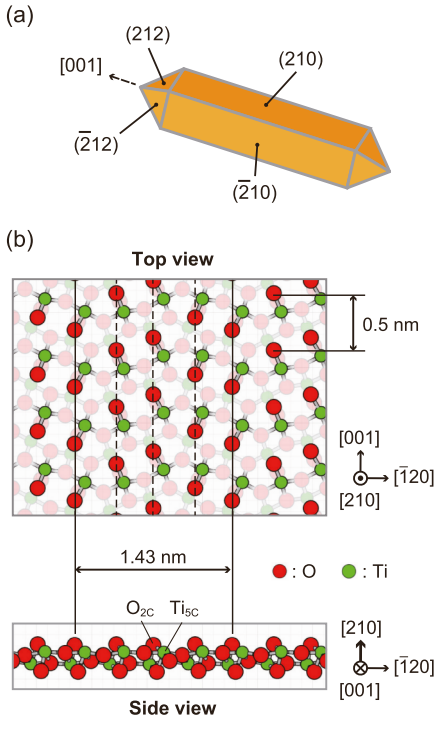

Figure 1. (a) Brookite TiO_2 nanorod with larger {210} and smaller {212} exposed crystal faces. (b) Atomic-scale models of brookite (210) surface (top and side views). Red and green colors indicate oxygen (O) and titanium (Ti) atoms, respectively. In the top view model, the topmost atoms are enhanced by depth fading display. The size of a repeating unit of atomic rows along [001] direction is 1.43 nm. Three additional atomic rows exist in the single repeating unit as indicated by dashed lines.

The first fixing method is based on the electrostatic attraction between brookite TiO_2 nanorods and muscovite mica. The cleaved surface of muscovite mica, which is widely used as the substrate for AFM measurements, has a negative charge at a wide range of pH values. A previous study reported that a mica surface is negatively charged even under pH 2 condition,[58] suggesting that the isoelectric point of the mica surface is lower than pH 2. If the brookite TiO_2 nanorods have positively charged surfaces, there is an electrostatic attraction (Coulombic attraction) between the brookite TiO_2 nanorods and the mica, as shown in Figure 2a. Zeta potential measurements were performed to investigate the surface charges of the brookite TiO_2 nanorods under different pH conditions (Figure 2b). The results suggest that the brookite TiO_2 nanorods have positively charged surfaces under acidic conditions (pH less than 6); the zeta potential increases with decreasing pH and reaches saturation at around pH 2. On the basis of the zeta potential measurements, an acidic aqueous suspension (pH 2) of brookite TiO_2 nanorods was used and was dropped onto the mica surface. As shown in Figure 2c, the adsorbed brookite TiO_2 nanorods prepared in an acidic aqueous suspension (pH 2) were stable during FM-AFM imaging in 0.1 M KCl aqueous solution. In contrast, the brookite TiO_2 nanorods deposited from a neutral aqueous suspension (pH 5) were not fixed on the substrate (see Figure 2d). The results show that the pH conditions are related to the adsorption step of TiO_2 nanorods onto the mica surface because the aqueous suspensions were only used for the adsorption step in this study. It is generally possible that the high salt concentration weakens electrostatic interactions between the brookite TiO_2 nanorods and mica. However, the adsorption structures of brookite TiO_2 nanorods that are prepared at pH 2 were stable even after the change of the solution from the adsorption solution (HCl, pH 2, <0.01 M) to the rinse solution (KCl, 0.1 M). We demonstrated that brookite TiO_2 nanorods in an acidic suspension (pH 2 in this study) can be fixed on mica via electrostatic attraction.

Figure 2e shows an FM-AFM image taken near the end of a brookite TiO_2 nanorod fixed by the electrostatic method. The characteristic shapes of the brookite TiO_2 nanorods were visualized in the AFM image, as indicated by the dotted lines in Figure 2e. The shapes in the AFM image agreed with those previously obtained by transmission electron microscopy.[51] We therefore assigned the crystal orientation of the brookite TiO_2 nanorods from the directions of the crystal shapes. As an initial step in the AFM imaging, we looked for brookite TiO_2 particles showing a rod shape and a flat side plane of (210) surfaces (see Figure S3 in the Supporting Information). After that, a tip was brought to the flat area of the brookite (210) surface and scanned with a reduced scan range. In this way, we acquired successive FM-AFM images in the order of Figures S3 and 2e,f to image the brookite (210) surfaces. An FM-AFM image of the (210) surface (Figure 2f) shows subnanometer-scale contrasts with striped structures parallel to the [001] direction. The periodic spacing of the striped structures (around 0.3 nm) shows good agreement with the distance between atomic rows of the topmost oxygen or titanium atoms (see Figure 1b). Here, we found slightly higher striped structures, with a periodicity of one out of four rows, as indicated by the black arrows in Figure 2f. The origin of the

DOI: 10.1021/acs.jpcc.8b06262
J. Phys. Chem. C 2018, 122, 24085−24093

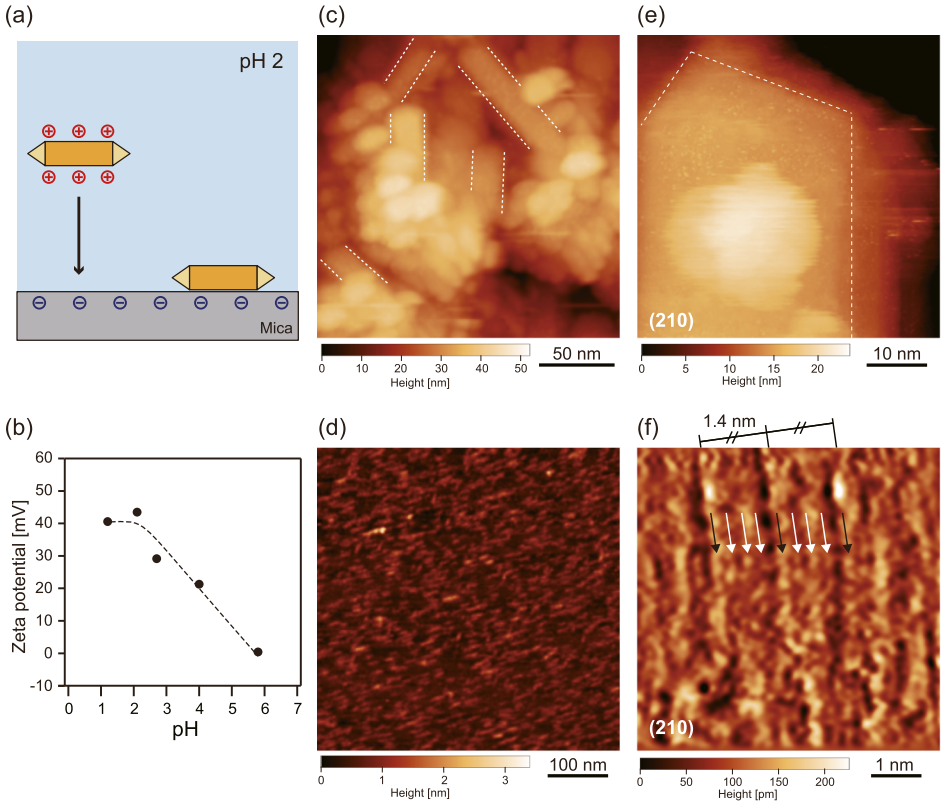

Figure 2. (a) Diagram of adsorption of TiO_2 nanorods on mica substrate at pH 2 by electrostatic method. (b) Zeta potentials of TiO_2 nanorods at various pH values. FM-AFM images of brookite TiO_2 nanorods prepared with (c) pH 2 and (d) 5 aqueous solutions. (e) FM-AFM image taken near end of brookite TiO_2 nanorod. (f) Atomic-resolution FM-AFM image of brookite (210) surface. Periodic contrasts with the spacing of 1.4 nm along [001] direction showed good agreement with the repeating unit of brookite TiO_2 crystal (see Figure 1b). White arrows indicate subnanometer-scale structures between the periodic contrasts with a 1.4 nm spacing that are visible only at the very limited area of the image. The dashed lines in (c,e) indicate the crystal shapes of brookite TiO_2 nanorods. All FM-AFM images were obtained in 0.1 M KCl aqueous solution.

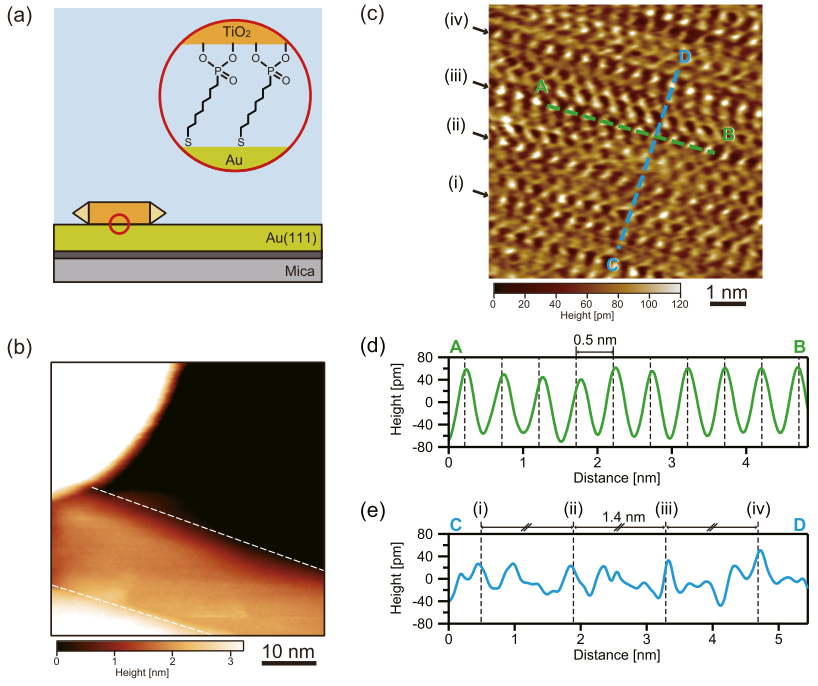

Figure 3. (a) Diagram of AFM sample preparation by cross-linking method. The inset shows the chemical cross-linking structures of phosphate-terminated alkanethiols between Au(111) substrate and brookite TiO_2 nanorods. (b) FM-AFM image of brookite TiO_2 nanorod. The dashed lines indicate the crystal shape of a brookite TiO_2 nanorod. (c) Atomic-resolution FM-AFM image of brookite (210) surface. (d,e) are height profiles along line AB and line CD in (c), respectively. All FM-AFM images were obtained in 0.1 M KCl aqueous solution.

DOI: 10.1021/acs.jpcc.8b06262
J. Phys. Chem. C 2018, 122, 24085−24093

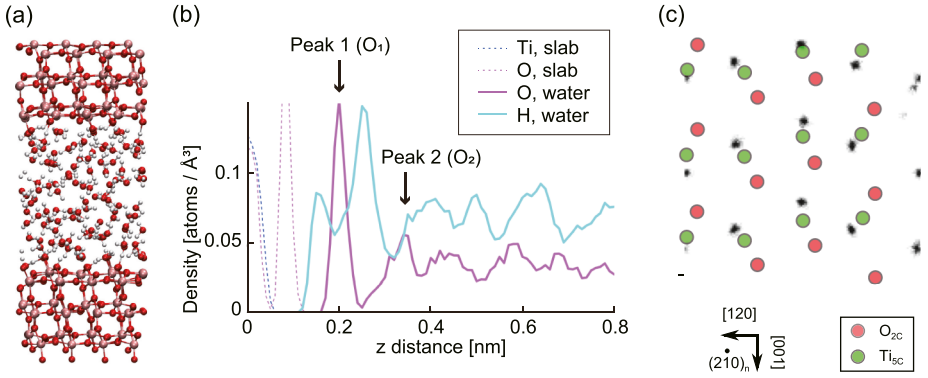

Figure 4. (a) Snap shot of atomistic model used for DFT MD simulation of brookite TiO_2(210)−water interface. (b) Vertical density profiles of oxygen (O) and titanium (Ti) atoms of brookite structures (slab) and oxygen (O) of water molecules. The two peaks of water molecules are defined as the first hydration structure (O_1) and second hydration structure (O_2), from the closest to the surface. (c) Lateral positions of topmost atoms and water molecules of first hydration layer. The darker spots represent the histogram of lateral positions of oxygens of water molecules within the first oxygen density peaks (O_1) of (b).

slightly higher striped structures at the (210) brookite surface cannot be explained by the crystal structure of brookite TiO_2 alone. We will discuss the possible origin later.

The FM-AFM images show atomically flat terraces and atomic-scale contrasts at the surface. In general, atomic-resolution AFM imaging of particle-shaped samples is very challenging because of the difficulties associated with particle fixation. There are therefore only a few reports of atomic-resolution AFM imaging of particle-shaped samples in liquid.[50] The results of this study show that an electrostatic fixing method can be used for atomic-resolution AFM imaging of the TiO_2 nanoparticles in liquid.

Covalent cross-linking is the second method used for fixing brookite TiO_2 nanorods for AFM measurements. The brookite TiO_2 nanorods were fixed with a SAM of a phosphate-terminated alkanethiol on an Au(111) substrate. Phosphate groups form covalent bonds with various metal oxides, including TiO_2, by the dehydration reaction. In this study, an alkanethiol SAM of 12-mercaptododecylphosphonic acid on Au(111) was used (Figure 3a) as the substrate. After spin-coating with a suspension of brookite TiO_2 nanorods, the substrate was heated at 120 °C for 24 h to accelerate the dehydration reaction between phosphate and the TiO_2 surface. Figure 3b shows an FM-AFM image of a brookite TiO_2 nanorod that was fixed on the phosphate-terminated SAM by covalent cross-linking. The nanorod shape of the brookite TiO_2 is visualized in the FM-AFM image. An atomic-resolution FM-AFM image of the brookite TiO_2 nanorods (Figure 3c) was obtained at the center of the nanorod, as shown in Figure 3b. The image (Figure 3c) shows rows consisting of periodic dot-like contrasts aligned in the [001] direction. As shown in Figure 3d, the periodic spacing of the dots in the [001] direction is 0.5 nm, which is consistent with the expected structures of the (210) brookite surface (see Figure 1b).

The quality of the AFM image (Figure 2f) obtained with the electrostatic method is lower than that obtained with the cross-linking method (Figure 3c). Here, we discuss a possible reason for the difference in the quality of subnanometer-scale AFM images between the two fixing methods. In general, conditions of the tip apex affect the quality of atomic-scale FM-AFM images. The estimated radius of the Si-coated tips used in this study was approximately 23 nm. This tip radius is much larger than an atomic scale. However, even with such a nanoscale tip, we are able to obtain atomic-scale FM-AFM images. The details of the imaging mechanism were previously reported.[45] In short, subnanometer-scale contrasts in the FM-AFM images obtained in liquid originate mainly from the free energy change caused by the events happening at the space between the tip front atom and the surface topmost atom. Therefore, atomic-scale FM-AFM images can be obtained even with a relatively blunt tip having a nanoscale radius. Meanwhile, the detailed patterns of the atomic-scale contrasts in the FM-AFM images are certainly affected by the structure and stability of the atomic-scale protrusion and the hydration structure formed under it. In our experiment with the samples prepared using the electrostatic method, it was difficult to find atomically flat surfaces of brookite (210) because of the large surface corrugation, as shown in Figure 2c. Thus, we speculate that the tip apex was contaminated or damaged during the tip scanning to find the flat (210) surfaces. In contrast, in the experiment with the samples prepared with the cross-linking method, it was relatively easy to find the atomically flat surfaces of brookite (210) owing to the small surface corrugations (see Figure S4 in the Supporting Information).

We found that some of the characteristic rows show a brighter contrast as indicated by arrows (i−iv) in Figure 3c. Although the regularity of the contrast is not perfect, the average distance between the rows with brighter contrast is 1.4 nm (Figure 3e). Such brighter rows with a spacing of 1.4 nm are also found in the FM-AFM image of the brookite TiO_2 nanorods fixed by the electrostatic method (Figure 2f). This agreement suggests that the bright rows correspond to the same structural feature.

The contrast formation mechanism in the subnanometer resolution FM-AFM images was investigated by performing DFT MD simulations of a brookite−water interface. Previous reports have indicated that not only the outermost atoms but also the hydration structures at the solid−liquid interface contribute to contrast formation in the subnanoscale FM-AFM images in water. Recently, Holmström et al. used the DFT MD simulations of brookite TiO_2−water interfaces to clarify the hydration structures and formation of OH-terminated structures at the surfaces in aqueous solutions.[52] In this study, the results of the FM-AFM experiments and DFT MD simulations were compared to determine the origin of the subnanoscale contrasts in the AFM images in water of brookite TiO_2(210) surfaces. Figure 4a shows a snapshot of the atomistic model used for the DFT MD simulations. The

DOI: 10.1021/acs.jpcc.8b06262
J. Phys. Chem. C 2018, 122, 24085−24093

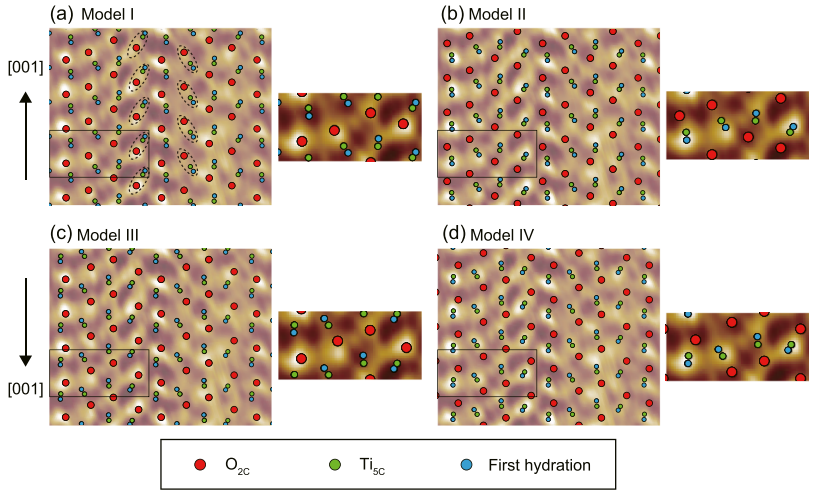

Figure 5. Four possible arrangements of topmost atoms and water molecules of first hydration layer for atomic-scale contrast in FM-AFM image. Positions of O_{2C} (a,c) and hydration structures (b,d) were adjusted to give bright contrasts of AFM image. Arrows with [001] indicate the directions of topmost atoms of brookite and hydration structures. Dashed lines in (a) indicate tilted contrasts in the AFM image.

simulations predict the spatial distribution of water molecules at the surface of brookite TiO_2(210). Two clear peaks appear in the vertical density profile of oxygens, as shown in Figure 4b. The results suggest that structured water molecules are present on the brookite TiO_2(210) surface. In this study, the two peaks are defined as the first hydration structure (O_1) and the second hydration structure (O_2) from the closest to the surface. Figure 4c shows the lateral positions of oxygen (O_{2C}), titanium (Ti_{5C}), and water molecules. The black distributions in Figure 4c indicate the lateral distributions of the oxygens of peak 1 (O_1). The simulation suggests that most of the water molecules in peak 1 were adsorbed on the surface, with formation of a chemical bond between a water, oxygen, and a surface Ti_{5C} ion. In addition, water molecules form hydrogen bonds with surface oxygens. The adsorption energy of a water molecule on brookite TiO_2(210) is 1.1 eV. As a result of stable interactions, lateral ordering of water molecules is observed in the first hydration layer (Figure 4c). In our previous study,[52] we have investigated the influence of ions (potassium and chloride ions) on hydration structures at the brookite−water interfaces by DFT MD simulation. According to this theoretical study, the lateral distribution of time-averaged hydration layers is not significantly affected by the existence of ions. Meanwhile, experimental results reported from different research groups demonstrated that atomic-scale contrasts in the 2D FM-AFM images of various surfaces obtained in an electrolytic solution can be largely explained by the arrangement of the surface topmost atoms and/or the hydration structures even without taking into account the influence of ions.[45,59−62]

As mentioned above, to clarify the origin of the subnanoscale contrasts obtained in water, the contributions from the topmost atoms (Ti_{5C} and O_{2C}) and the hydration structures should be taken into account. The bright particle-like contrasts therefore probably arise from the first hydration structures or the topmost oxygen atoms (O_{2C}). Two possibilities (oxygen atoms or first hydration structures) remain as possible origins of the subnanoscale contrast. In addition, a unique assignment of the [001] direction in the FM-AFM image is impossible on the basis of only the obtained data. Four possible models therefore remain for assignment of the subnanoscale contrasts to the surface structures, as shown in Figure 5. In models I and III, the positions of the oxygen atoms and the bright particle-like contrasts are superimposed. Models II and IV show superimposed images of water molecules in the first hydration structures and the bright contrasts. In some atomic rows, the tilted contrasts in the FM-AFM image agree well with the arrangement of adjacent Ti−O-hydration pairs, as indicated by the dashed lines. Although it is difficult to assign a definite arrangement from the four possible candidates, the bright particle-like contrasts are more likely to originate from the first hydration structures. In a previous FM-AFM investigations of calcite in water,[63] subnanoscale contrasts were formed by scanning a tip on the first hydration structures because of the high adsorption energy of water molecules on calcite (approximately 1 eV). The adsorption energy of water molecules on brookite TiO_2(210) (1.1 eV) is comparable to that on calcite. These results suggest that the tip is scanned on the first hydration structures when subnanoscale contrasts of brookite TiO_2(210) are formed.

For the bright rows, we were unable to determine the contrast formation mechanism even from the results of the DFT MD simulation. One possible model is OH termination at the brookite (210) surface by dissociative adsorption of water. Although adsorption of water molecules in the dissociated state was observed in the DFT MD simulation, it was impossible to obtain statistical data to investigate this as the possible origin of the bright rows observed in the FM-AFM images because of the huge computational costs. As another possible origin of the bright rows, it may be caused by the influence of ions. However, it is very difficult to quantitatively estimate the influence of ions with our present results. Although further studies are needed to determine the origin, the atomic-scale FM-AFM images suggest the presence of characteristic structures with a regularity of one in four rows at the brookite (210) surfaces.

CONCLUSIONS

In this study, we established two fixing methods to enable the AFM investigations of brookite TiO_2 nanoparticles in liquid. The two fixing methods were used for visualization of atomic-scale surface structures of brookite (210). The visualization mechanisms were investigated by calculating the distributions

DOI: 10.1021/acs.jpcc.8b06262
J. Phys. Chem. C 2018, 122, 24085−24093

of the topmost atoms and hydration water molecules at the interface by DFT MD simulations. Comparisons of the subnanoscale contrasts in the FM-AFM images and the distribution of the topmost atoms and water molecules showed that the subnanoscale contrasts originated from the first hydration structures or the topmost oxygen atoms. Moreover, although the origin was not completely clear, we found the presence of bright rows of particle-like contrasts with a periodicity of one out of four rows at the interface between brookite (210) and water. The established fixing methods help to improve our understanding of the photocatalytic reactions of TiO_2, not only brookite but also rutile and anatase.

■ ASSOCIATED CONTENT

Supporting Information

The Supporting Information is available free of charge on the ACS Publications website at DOI: 10.1021/acs.jpcc.8b06262.

SEM image and XRD patterns of the prepared brookite TiO_2 nanorods and the AFM image of a sample prepared with the cross-linking method (PDF)

■ AUTHOR INFORMATION

Corresponding Authors

*E-mail: adam.foster@aalto.fi (A.S.F.).
*E-mail: fukuma@staff.kanazawa-u.ac.jp (T.F.).

ORCID

Adam S. Foster: 0000-0001-5371-5905
Takeshi Fukuma: 0000-0001-8971-6002

Notes

The authors declare no competing financial interest.

■ ACKNOWLEDGMENTS

This work was supported by ACT-C, Japan Science and Technology Agency, and World Premier International Research Center Initiative (WPI), MEXT, Japan. We acknowledge financial support by the Academy of Finland through the Centres of Excellence Program (project no. 251748). H.A. acknowledges financial support from JST PRESTO (grant number JPMJPR1411), Japan. E.H. acknowledges financial support from the Emil Aaltonen foundation. We acknowledge that the results of this research have been achieved using the DECI resource Beskow based in Sweden at PDC/KTH with support from the PRACE aisbl. We also acknowledge CSC-IT Center for Science, Finland, for computational resources and application support.

■ REFERENCES

(1) Li, Z.; Cong, S.; Xu, Y. Brookite vs anatase TiO2 in the photocatalytic activity for organic degradation in water. *ACS Catal.* **2014**, *4*, 3273−3280.

(2) Mattsson, A.; Österlund, L. Adsorption and photoinduced decomposition of acetone and acetic acid on anatase, brookite, and rutile TiO2 nanoparticles. *J. Phys. Chem. C* **2010**, *114*, 14121−14132.

(3) Schneider, J.; Matsuoka, M.; Takeuchi, M.; Zhang, J.; Horiuchi, Y.; Anpo, M.; Bahnemann, D. W. Understanding TiO2 photocatalysis: Mechanisms and materials. *Chem. Rev.* **2014**, *114*, 9919−9986.

(4) Rodriguez, M. M.; Peng, X.; Liu, L.; Li, Y.; Andino, J. M. A density functional theory and experimental study of CO2 interaction with brookite TiO2. *J. Phys. Chem. C* **2012**, *116*, 19755−19764.

(5) Ohno, T.; Higo, T.; Saito, H.; Yuajn, S.; Jin, Z.; Yang, Y.; Tsubota, T. Dependence of photocatalytic activity on aspect ratio of a brookite TiO2 nanorod and drastic improvement in visible light responsibility of a brookite TiO2 nanorod by site-selective modification of Fe3+ on exposed faces. *J. Mol. Catal. A: Chem.* **2015**, *396*, 261−267.

(6) Zhao, H.; Liu, L.; Andino, J. M.; Li, Y. Bicrystalline TiO2 with controllable anatase-brookite phase content for enhanced CO2 photoreduction to fuels. *J. Mater. Chem. A* **2013**, *1*, 8209−8216.

(7) Guo, M.; Li, L.; Lin, H.; Zuo, Y.; Huang, X.; Li, G. Targeted deposition of ZnO2 on brookite TiO2 nanorods towards high photocatalytic activity. *Chem. Commun.* **2013**, *49*, 11752−11754.

(8) Lin, H.; Li, L.; Zhao, M.; Huang, X.; Chen, X.; Li, G.; Yu, R. Synthesis of high-quality brookite TiO2 single-crystalline nanosheets with specific facets exposed: Tuning catalysts from inert to highly reactive. *J. Am. Chem. Soc.* **2012**, *134*, 8328−8331.

(9) Kandiel, T. A.; Feldhoff, A.; Robben, L.; Dillert, R.; Bahnemann, D. W. Tailored titanium dioxide nanomaterials: Anatase nanoparticles and brookite nanorods as highly active photocatalysts. *Chem. Mater.* **2010**, *22*, 2050−2060.

(10) Murakami, N.; Kamai, T.; Tsubota, T.; Ohno, T. Novel hydrothermal preparation of pure brookite-type titanium(IV) oxide nanocrystal under strong acidic conditions. *Catal. Commun.* **2009**, *10*, 963−966.

(11) Reyes-Coronado, D.; Rodríguez-Gattorno, G.; Espinosa-Pesqueira, M. E.; Cab, C.; de Coss, R.; Oskam, G. Phase-pure TiO2 nanoparticles: anatase, brookite and rutile. *Nanotechnology* **2008**, *19*, 145605.

(12) Deng, Q.; Wei, M.; Ding, X.; Jiang, L.; Ye, B.; Wei, K. Brookite-type TiO2 nanotubes. *Chem. Commun.* **2008**, 3657−3659.

(13) Buonsanti, R.; Grillo, V.; Carlino, E.; Giannini, C.; Kipp, T.; Cingolani, R.; Cozzoli, P. D. Nonhydrolytic synthesis of high-quality anisotropically shaped brookite TiO2 nanocrystals. *J. Am. Chem. Soc.* **2008**, *130*, 11223−11233.

(14) Li, J.-G.; Ishigaki, T.; Sun, X. Anatase, brookite, and rutile nanocrystals via redox reactions under mild hydrothermal conditions: Phase-selective synthesis and physicochemical properties. *J. Phys. Chem. C* **2007**, *111*, 4969−4976.

(15) Giessibl, F. J.; Hembacher, S.; Bielefeldt, H.; Mannhart, J. Subatomic features on the silicon (111)-(7×7) surface observed by atomic force microscopy. *Science* **2000**, *289*, 422−425.

(16) Bennewitz, R.; Pfeiffer, O.; Schär, S.; Barwich, V.; Meyer, E.; Kantorovich, L. N. Atomic corrugation in nc-AFM of alkali halides. *Appl. Surf. Sci.* **2002**, *188*, 232−237.

(17) Zhang, J.; Zhou, P.; Liu, J.; Yu, J. New understanding of the difference of photocatalytic activity among anatase, rutile and brookite TiO2. *Phys. Chem. Chem. Phys.* **2014**, *16*, 20382−20386.

(18) Li, W.-K.; Gong, X.-Q.; Lu, G.; Selloni, A. Different reactivities of TiO2 polymorphs: Comparative DFT calculations of water and formic acid adsorption at anatase and brookite TiO2 surfaces. *J. Phys. Chem. C* **2008**, *112*, 6594−6596.

(19) Gong, X.-Q.; Selloni, A. First-principles study of the structures and energetics of stoichiometric brookite TiO2 surfaces. *Phys. Rev. B: Condens. Matter Mater. Phys.* **2007**, *76*, 235307.

(20) Onoda, J.; Pang, C. L.; Yurtsever, A.; Sugimoto, Y. Subsurface charge repulsion of adsorbed H-adatoms on TiO2 (110). *J. Phys. Chem. C* **2014**, *118*, 13674−13679.

(21) Yurtsever, A.; Fernandez-Torre, D.; González, C.; Jelínek, P.; Pou, P.; Sugimoto, Y.; Abe, M.; Pérez, R.; Morita, S. Understanding image contrast formation in TiO2 with force spectroscopy. *Phys. Rev. B: Condens. Matter Mater. Phys.* **2012**, *85*, 125416.

(22) Lauritsen, J. V.; Reichling, M. Atomic resolution non-contact atomic force microscopy of clean metal oxide surfaces. *J. Phys.: Condens. Matter* **2010**, *22*, 263001.

(23) Greuling, A.; Rahe, P.; Kaczmarski, M.; Kühnle, A.; Rohlfing, M. Combined NC-AFM and DFT study of the adsorption geometry of trimesic acid on rutile TiO2 (110). *J. Phys.: Condens. Matter* **2010**, *22*, 345008.

(24) Altman, E. I.; Schwarz, U. D. Mechanisms, kinetics, and dynamics of oxidation and reactions on oxide surfaces investigated by scanning probe microscopy. *Adv. Mater.* **2010**, *22*, 2854−2869.

DOI: 10.1021/acs.jpcc.8b06262
J. Phys. Chem. C 2018, 122, 24085−24093

(25) Hiasa, T.; Kimura, K.; Onishi, H.; Ohta, M.; Watanabe, K.; Kokawa, R.; Oyabu, N.; Kobayashi, K.; Yamada, H. Solution-TiO2 interface probed by frequency-modulation atomic force microscopy. *Jpn. J. Appl. Phys.* **2009**, *48*, 08JB19.
(26) Enevoldsen, G. H.; Pinto, H. P.; Foster, A. S.; Jensen, M. C.; Hofer, W. A.; Hammer, B.; Lauritsen, J. V.; Besenbacher, F. Imaging of the hydrogen subsurface site in rutile TiO2. *Phys. Rev. Lett.* **2009**, *102*, 136103.
(27) Enevoldsen, G. H.; Pinto, H. P.; Foster, A. S.; Jensen, M. C. R.; Kühnle, A.; Reichling, M.; Hofer, W. A.; Lauritsen, J. V.; Besenbacher, F. Detailed scanning probe microscopy tip models determined from simultaneous atom-resolved AFM and STM studies of the TiO2 (110) surface. *Phys. Rev. B: Condens. Matter Mater. Phys.* **2008**, *78*, 045416.
(28) Enevoldsen, G. H.; Foster, A. S.; Christensen, M. C.; Lauritsen, J. V.; Besenbacher, F. Noncontact atomic force microscopy studies of vacancies and hydroxyls of TiO2 (110): Experiments and atomistic simulations. *Phys. Rev. B: Condens. Matter Mater. Phys.* **2007**, *76*, 205415.
(29) Sasahara, A.; Pang, C. L.; Onishi, H. Probe Microscope Observation of Platinum Atoms Deposited on the TiO2(110)-(1 × 1) Surface. *J. Phys. Chem. B* **2006**, *110*, 13453−13457.
(30) Pang, C. L.; Sasahara, A.; Onishi, H.; Chen, Q.; Thornton, G. Noncontact atomic force microscopy imaging of water dissociation products on TiO2 (110). *Phys. Rev. B: Condens. Matter Mater. Phys.* **2006**, *74*, 073411.
(31) Sasahara, A.; Kitamura, S.-i.; Uetsuka, H.; Onishi, H. Oxygen-atom vacancies imaged by a noncontact atomic force microscope operated in an atmospheric pressure of N2 gas. *J. Phys. Chem. B* **2004**, *108*, 15735−15737.
(32) Tero, R.; Fukui, K.-i.; Iwasawa, Y. Atom-resolved surface structures and molecular adsorption on TiO2 (001) investigated by scanning tunneling microscopy. *J. Phys. Chem. B* **2003**, *107*, 3207−3214.
(33) Foster, A. S.; Pakarinen, O. H.; Airaksinen, J. M.; Gale, J. D.; Nieminen, R. M. Simulating atomic force microscopy imaging of the ideal and defected TiO2 (110) surface. *Phys. Rev. B: Condens. Matter Mater. Phys.* **2003**, *68*, 195410.
(34) Tanner, R. E.; Sasahara, A.; Liang, Y.; Altman, E. I.; Onishi, H. Formic acid adsorption on anatase TiO2 (001)-(1×4) thin films studied by NC-AFM and STM. *J. Phys. Chem. B* **2002**, *106*, 8211−8222.
(35) Ke, S. H.; Uda, T.; Terakura, K. STM-AFM image formation on TiO2 (110) 1×1 and 1×2 surfaces. *Appl. Surf. Sci.* **2002**, *188*, 319−324.
(36) Ashino, M.; Sugawara, Y.; Morita, S.; Ishikawa, M. Atomic resolution noncontact atomic force and scanning tunneling microscopy of TiO2 (110)-(1×1) and -(1×2): Simultaneous imaging of surface structures and electronic states. *Phys. Rev. Lett.* **2001**, *86*, 4334−4337.
(37) Fukui, K.-i.; Onishi, H.; Iwasawa, Y. Atom-resolved image of the TiO2 (110) surface by noncontact atomic force microscopy. *Phys. Rev. Lett.* **1997**, *79*, 4202−4205.
(38) Stetsovych, O.; Todorović, M.; Shimizu, T. K.; Moreno, C.; Ryan, J. W.; León, C. P.; Sagisaka, K.; Palomares, E.; Matolín, V.; Fujita, D.; et al. Atomic species identification at the (101) anatase surface by simultaneous scanning tunnelling and atomic force microscopy. *Nat. Commun.* **2015**, *6*, 7265.
(39) Di Paola, A.; Bellardita, M.; Palmisano, L. Brookite, the Least Known TiO2 Photocatalyst. *Catalysts* **2013**, *3*, 36−73.
(40) Lu, Y.; Jaeckel, B.; Parkinson, B. A. Preparation and characterization of terraced surfaces of low-index faces of anatase, rutile, and brookite. *Langmuir* **2006**, *22*, 4472−4475.
(41) Fukuma, T.; Kimura, M.; Kobayashi, K.; Matsushige, K.; Yamada, H. Development of low noise cantilever deflection sensor for multienvironment frequency-modulation atomic force microscopy. *Rev. Sci. Instrum.* **2005**, *76*, 053704.
(42) Fukuma, T.; Jarvis, S. P. Development of liquid-environment frequency modulation atomic force microscope with low noise deflection sensor for cantilevers of various dimensions. *Rev. Sci. Instrum.* **2006**, *77*, 043701.
(43) Fukuma, T. Wideband low-noise optical beam deflection sensor with photothermal excitation for liquid-environment atomic force microscopy. *Rev. Sci. Instrum.* **2009**, *80*, 023707.
(44) Kitta, M.; Kohyama, M.; Onishi, H. True atomic-scale imaging of a spinel Li4Ti5O12 (111) surface in aqueous solution by frequency-modulation atomic force microscopy. *Appl. Phys. Lett.* **2014**, *105*, 111606.
(45) Fukuma, T.; Reischl, B.; Kobayashi, N.; Spijker, P.; Canova, F. F.; Miyazawa, K.; Foster, A. S. Mechanism of atomic force microscopy imaging of three-dimensional hydration structures at a solid-liquid interface. *Phys. Rev. B: Condens. Matter Mater. Phys.* **2015**, *92*, 155412.
(46) Asakawa, H.; Ikegami, K.; Setou, M.; Watanabe, N.; Tsukada, M.; Fukuma, T. Submolecular-scale imaging of α-helices and C-terminal domains of tubulins by frequency modulation atomic force microscopy in liquid. *Biophys. J.* **2011**, *101*, 1270−1276.
(47) Ido, S.; Kimiya, H.; Kobayashi, K.; Kominami, H.; Matsushige, K.; Yamada, H. Immunoactive two-dimensional self-assembly of monoclonal antibodies in aqueous solution revealed by atomic force microscopy. *Nat. Mater.* **2014**, *13*, 264−270.
(48) Sasahara, A.; Tomitori, M. Frequency modulation atomic force microscope observation of TiO2 (110) surfaces in water. *J. Vac. Sci. Technol., B: Nanotechnol. Microelectron.: Mater., Process., Meas., Phenom.* **2010**, *28*, C4C5−C4C10.
(49) Chiodini, S.; Reinares-Fisac, D.; Espinosa, F. M.; Gutierrez-Puebla, E.; Monge, A.; Gándara, F.; Garcia, R. Angstrom-resolved metal-organic framework-liquid interfaces. *Sci. Rep.* **2017**, *7*, 11088.
(50) Imada, H.; Kimura, K.; Onishi, H. Atom-resolved AFM imaging of calcite nanoparticles in water. *Chem. Phys.* **2013**, *419*, 193−195.
(51) Zhang, L.; Menendez-Flores, V. M.; Murakami, N.; Ohno, T. Improvement of photocatalytic activity of brookite titanium dioxide nanorods by surface modification using chemical etching. *Appl. Surf. Sci.* **2012**, *258*, 5803−5809.
(52) Holmström, E.; Ghan, S.; Asakawa, H.; Fujita, Y.; Fukuma, T.; Kamimura, S.; Ohno, T.; Foster, A. S. Hydration structure of brookite TiO2 (210). *J. Phys. Chem. C* **2017**, *121*, 20790−20801.
(53) Inada, N.; Asakawa, H.; Matsumoto, Y.; Fukuma, T. Molecular-scale surface structures of oligo(ethylene glycol)-terminated self-assembled monolayers investigated by frequency modulation atomic force microscopy in aqueous solution. *Nanotechnology* **2014**, *25*, 305602.
(54) Akrami, S. M. R.; Nakayachi, H.; Watanabe-Nakayama, T.; Asakawa, H.; Fukuma, T. Significant improvements in stability and reproducibility of atomic-scale atomic force microscopy in liquid. *Nanotechnology* **2014**, *25*, 455701.
(55) Perdew, J. P.; Burke, K.; Ernzerhof, M. Generalized gradient approximation made simple. *Phys. Rev. Lett.* **1996**, *77*, 3865−3868.
(56) Grimme, S.; Antony, J.; Ehrlich, S.; Krieg, H. A consistent and accurate ab initio parametrization of density functional dispersion correction (DFT-D) for the 94 elements H-Pu. *J. Chem. Phys.* **2010**, *132*, 154104.
(57) CP2K software package. http://www.cp2k.org (accessed Aug 24, 2018).
(58) Nishimura, S.; Tateyama, H.; Tsunematsu, K.; Jinnai, K. Zeta potential measurement of muscovite mica basal plane-aqueous solution interface by means of plane interface technique. *J. Colloid Interface Sci.* **1992**, *152*, 359−367.
(59) Fukuma, T.; Ueda, Y.; Yoshioka, S.; Asakawa, H. Atomic-scale distribution of water molecules at the mica-water interface visualized by three-dimensional scanning force microscopy. *Phys. Rev. Lett.* **2010**, *104*, 016101.
(60) Kobayashi, K.; Oyabu, N.; Kimura, K.; Ido, S.; Suzuki, K.; Imai, T.; Tagami, K.; Tsukada, M.; Yamada, H. Visualization of hydration layers on muscovite mica in aqueous solution by frequency-modulation atomic force microscopy. *J. Chem. Phys.* **2013**, *138*, 184704.
(61) Tracey, J.; Miyazawa, K.; Spijker, P.; Miyata, K.; Reischl, B.; Canova, F. F.; Rohl, A. L.; Fukuma, T.; Foster, A. S. Understanding

DOI: 10.1021/acs.jpcc.8b06262
J. Phys. Chem. C 2018, 122, 24085−24093

2D atomic resolution imaging of the calcite surface in water by frequency modulation atomic force microscopy. *Nanotechnology* **2016**, *27*, 415709.

(62) Ito, F.; Kobayashi, K.; Spijker, P.; Zivanovic, L.; Umeda, K.; Nurmi, T.; Holmberg, N.; Laasonen, K.; Foster, A. S.; Yamada, H. Molecular resolution of the water interface at an alkali halide with terraces and steps. *J. Phys. Chem. C* **2016**, *120*, 19714−19722.

(63) Miyata, K.; Tracey, J.; Miyazawa, K.; Haapasilta, V.; Spijker, P.; Kawagoe, Y.; Foster, A. S.; Tsukamoto, K.; Fukuma, T. Dissolution processes at step edges of calcite in water investigated by high-speed frequency modulation atomic force microscopy and simulation. *Nano Lett.* **2017**, *17*, 4083−4089.

DOI: 10.1021/acs.jpcc.8b06262
J. Phys. Chem. C 2018, 122, 24085−24093